APS physics

CHORUS

This is the accepted manuscript made available via CHORUS. The article has been published as:

Effect of magnetic field and chemical potential on the RKKY interaction in the math xmlns="http://www.w3.org/1998/Math/MathML">mi>α/mi> mtext>−/mtext>msub>mi mathvariant="script">T /mi>mn>3/mn>/msub>/math> lattice

Oleksiy Roslyak, Godfrey Gumbs, Antonios Balassis, and Heba Elsayed

Phys. Rev. B **103**, 075418 — Published 12 February 2021

DOI: 10.1103/PhysRevB.103.075418

Effect of magnetic field and chemical potential on the RKKY interaction in the α-$\mathcal{T}_3$ lattice

Oleksiy Roslyak,[1] Godfrey Gumbs,[2] Antonios Balassis,[1] and Heba Elsayed[1]
[1] *Department of Physics & Engineering Physics, Fordham University, 441 East Fordham Road, Bronx, NY 10458 USA and*
[2] *Department of Physics and Astronomy, Hunter College of the City University of New York, 695 Park Avenue, New York, NY 10065, USA*

The interaction energy for the indirect-exchange or Ruderman-Kittel-Kasuva-Yosida (RKKY) interaction between magnetic spins localized on lattice sites of the α-$\mathcal{T}_3$ model is calculated using linear response theory. In this model, the AB-honeycomb lattice structure is supplemented with C atoms at the centers of the hexagonal lattice. This introduces a parameter α for the ratio of the hopping integral from hub-to-rim and that around the rim of the hexagonal lattice. A valley and α-dependent retarded Greens function matrix is used to form the susceptibility. Analytic and numerical results are obtained for undoped α-$\mathcal{T}_3$, when the chemical potential is finite and also in the presence of an applied magnetic field. We demonstrate the anisotropy of these results when the magnetic impurities are placed on the A,B and C sublattice sites. Additionally, comparison of the behavior of the susceptibility of α-$\mathcal{T}_3$ with graphene shows that there is a phase transition at $\alpha = 0$.

I. INTRODUCTION

An effective single-particle model Hamiltonian representing an electronic crystal has been recently constructed to represent the low-lying Bloch band of the α-$\mathcal{T}_3$ lattice (for a review of artificial flat band systems, see Ref. [1]). The electronic properties of this material have come under growing scrutiny for a number of important reasons which are fundamental and technological [2–22]. The potential tunability of these materials ranging from their optical and transport properties to their response to a uniform magnetic field and varying chemical potential presents researchers with the opportunity to investigate new materials. Regarding their fabrication, it was suggested in [2] that an α-$\mathcal{T}_3$ lattice may be constructed with the use of cold fermionic atoms confined to an optical lattice with the help of three pairs of laser beams for the optical dice ($\alpha = 1$) lattice [23]. Jo, et al. [9] successfully fabricated a two-dimensional kagome lattice consisting of ultra-cold atoms by superimposing a triangular optical lattice on another one commensurate with it, and generated by light at specified wavelengths. The α-$\mathcal{T}_3$ and kagome lattices are related in that they both have flat bands as well as Dirac cones at low energies. In modeling this structure, an AB-honeycomb lattice like that in graphene is combined with C atoms at the centers of the hexagonal lattice as depicted in Fig. 1. Consequently, a parameter α is introduced to represent the ratio of the hopping integral between the hub and the rim (αt) to that around the rim (t) of the hexagonal lattice. When one of the three pairs of laser beams is dephased, it is proposed in [23] that this could allow the possible variation of the hopping parameter over the range $0 < \alpha \leq 1$.

Interestingly, it would be informative to explore how the optical and transport properties of α-$\mathcal{T}_3$ systems are affected by defects. These include substituting impurities or guest atoms in a hexagonal lattice with fermionic host

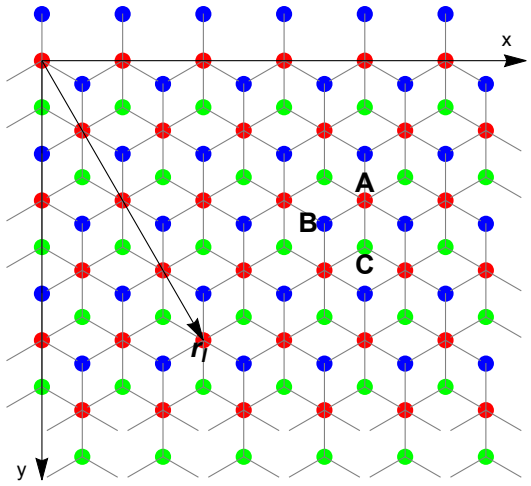

FIG. 1: (Color online) Lattice sites of the $\alpha - \mathcal{T}_3$ model. The "rim" atoms are labeled A and B whereas C is a "hub" atom.

atoms. In this way, one could effectively manipulate the fundamental properties which are inherent to the α-$\mathcal{T}_3$ system. The guest atoms could be added to their hosts by chemical vapor deposition (CVD) or discharge experiments. With doping, the A and B sublattices are no longer equivalent since the π bonding on these lattices may be seriously distorted and this causes significant modification of the physical properties, including the energy band structure with a deviation from the original Dirac cone and flat band. However, at low doping ($< 1.5\%$), the low-energy portion of the band structure is only slightly affected. We emphasize that the doping configuration and concentration in general create unusual band structures with feature-rich and unique properties.

Oriekhov and Gusynin [15] took the first step of investigating the role played by the sea of background α-$\mathcal{T}_3$-fermions on the indirect exchange interaction between a

pair of spins localized on lattice sites. Local moments like these may occur near extended defects. The doping giving rise to the presence of these spins was assumed to have such a low concentration that the energy dispersion and the zero band gap stay unaltered. Specifically, these authors [15] were interested in this effect of doping and temperature on the Ruderman-Kittel-Kasuva-Yosida (RKKY) or indirect-exchange coupling as it was discussed for different types of two-dimensional (2D) materials by others [24–28] between spins via the host conduction electrons of free standing mono-layer graphene, [29–39] and biased single-layer silicene [40]. In this paper, we continue the investigation in [15] by calculating the effect of a uniform magnetic field and a variable chemical potential on the RKKY interaction of α-$\mathcal{T}_3$. It is worthwhile getting a better understanding of the behavior of this topic since one could exploit the RKKY interaction to determine spin ordering as excitations near the Fermi level are in part governed by the indirect exchange interaction between local magnetic moments [41–43].

The rest of this paper is organized as follows. In Sec. II, we present the low-energy α-$\mathcal{T}_3$ model Hamiltonian and derive the lattice Green's functions for small magnetic field (Zeeman effect). We calculate the indirect exchange coupling between a pair of impurities. We represent the RKKY interaction energy as a Hadamard product of three matrices: a valley matrix, an $\alpha-$matrix and a distance matrix. In Sec. III, we present numerical results for the α-dependent exchange interaction in the case of strong magnetic field when Landau levels have been formed. We demonstrate that the spin susceptibility for the α-$\mathcal{T}_3$ model is different in nature from that for graphene, thereby signaling a magnetic phase transition at $\alpha = 0$. We also analyze the behavior of the spin susceptibility at low and high doping. We conclude with a summary in Sec. IV.

II. WEAK MAGNETIC FIELD: ZEEMAN EFFECT ON RKKY INTERACTION FOR THE α-$\mathcal{T}_3$ MODEL.

The conventional α-$\mathcal{T}_3$ model describes triplon energy bands. A small magnetic field induces nontrivial topological character in the triplon energy spectrum. First, we shall introduce the lattice specific Green's functions which are essential for calculating RKKY interactions. Throughout the paper, we use two conventions for the notation adopted: bold capitalized letters stand for 3×3 matrices (or 3×1 vectors); tilded quantities are dimensionless. The energy spectrum can be derived from the low-energy Hamiltonian at the $\mathbf{K}$ and $\mathbf{K}'$ points,

$$\mathbf{H} = \begin{pmatrix} \Delta & f_{\lambda,\mathbf{k}}\cos\phi & 0 \\ f^*_{\lambda,\mathbf{k}}\cos\phi & 0 & f_{\lambda,\mathbf{k}}\sin\phi \\ 0 & f^*_{\lambda,\mathbf{k}}\sin\phi & -\Delta \end{pmatrix}, \qquad (1)$$

where $0 < \phi \leq \pi/4$ is the hopping parameter with $\alpha = \tan\phi$, $f_{\lambda,\mathbf{k}} = \lambda\epsilon_k\ e^{-i\lambda\theta_k}$ with $\epsilon_k = \hbar v_F k$; $\lambda = \pm 1$ stands for the valley index at the $\mathbf{K}$ and $\mathbf{K}'$ points located at $\left(\lambda\frac{4\pi}{3\sqrt{3}a}, 0\right)$, a is the conventional graphene carbon-carbon distance and v_F stands for the Fermi velocity. The angle between $\mathbf{k}$ and the $x-$axis is given by θ_k yielding $k_x/|\mathbf{k}| = \cos\theta_k$, $k_y/|\mathbf{k}| = \sin\theta_k$. The rows and columns of the Hamiltonian are labeled by the (`A,B,C`) lattice indices indicated in Fig. 1. The mass term induced by the pseudo-magnetic field as it follows from Ref. [45] is denoted by $\Delta = mv_F^2/2$.

The energy spectrum corresponding to Eq. (1) first reported in Ref. [46] is shown in Fig. 2. For convenience, we denote by $\omega = E/E_0$ and $\delta = \Delta/E_0$ the normalized energy and normalized gap respectively where $E_0 = \hbar v_F/a$. In the absence of magnetic field, the triplon is built of two Dirac cones as well as a "flat band". For the dice lattice $\phi = \pi/4$ and the effect of the mass term is to open a gap at $k = 0$ such as $-\delta \leq \omega \leq \delta$ and we recover the standard spin-1 dispersion. This also breaks time reversal symmetry. Reducing the value in ϕ we shall obtain two non-symmetrical gaps $0 < \omega \leq \delta$ and $-\delta \leq \omega \leq \omega_\delta$, where $\omega_\delta = -\delta\cos(2\phi)$ (asymptotic value of the middle). The bending of the flat band reveals the non-triviality of the energy dispersion topology and may be related to a nonzero Chern number. One of the most striking features of the α-$\mathcal{T}_3$ model is the broken particle-hole symmetry.

We define the Green's functions by the elements of an inverse matrix involving the energy difference with the Hamiltonian of Eq. (1) as

$$\begin{aligned} \mathbf{G}(\mathbf{k}, E; \lambda; \phi) &= \left[(E + i0^+)\mathbf{I} - \mathbf{H}\right]^{-1} \qquad (2) \\ &= \begin{pmatrix} G_{\mathtt{AA}} & G_{\mathtt{AB}} & G_{\mathtt{AC}} \\ G^*_{\mathtt{AB}} & G_{\mathtt{BB}} & G_{\mathtt{BC}} \\ G^*_{\mathtt{AC}} & G^*_{\mathtt{BC}} & G_{\mathtt{CC}} \end{pmatrix}. \end{aligned}$$

In this notation, $\mathbf{I}$ is the unit matrix and the replacement $E \to E + i0^+$ guarantees the retarded nature of the Green's functions. The direct diagonalization of the Green's tensor yields

$$\mathbf{G}(\mathbf{k}, E; \lambda; \phi) = \mathcal{D}^{-1}\begin{pmatrix} E(E+\Delta) - \epsilon_k^2\sin^2\phi & (E+\Delta)f_{\lambda,\mathbf{k}}\cos\phi & f^2_{\lambda,\mathbf{k}}\sin(2\phi)/2 \\ & E^2 - \Delta^2 & (E-\Delta)f_{\lambda,\mathbf{k}}\sin\phi \\ & & E(E-\Delta) - \epsilon_k^2\cos^2\phi \end{pmatrix}, \qquad (3)$$

with the determinant given by $\mathcal{D}(\mathbf{k}, E) = E\left(E^2 - \Delta^2\right) - \left[E + \Delta\cos(2\phi)\right]\epsilon_k^2$, whose dispersion is given by its poles as

shown in Fig. 2.

Clearly, the Green's function matrix is Hermitian and we observe that $G_{\mathtt{BB}}(\mathbf{k}, E; \lambda; \phi) = G_{\mathtt{AA}}(\mathbf{k}, E; \lambda; \phi = 0)$ is the only element of the Green's function matrix which does not depend on ϕ. Consequently, this leads to RKKY interaction between spins on the B site to be unaffected when ϕ is varied.

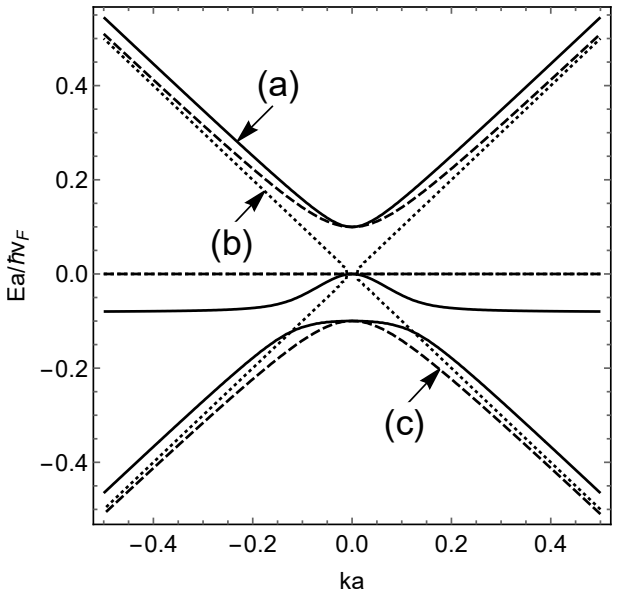

FIG. 2: Dispersion of (a) massive $\Delta a/\hbar v_F = 0.1$ triplon with $\phi = \pi/10$; (b) masless $\Delta a/\hbar v_F = 0$ triplon with $\phi = \pi/10$; (c) massive $\Delta a/\hbar v_F = 0.1$ spin-1 fermions (dice lattice) with $\phi = \pi/4$. Changing the magnetic filed orientation $B_z \to -B_z$, or in other words $\Delta \to -\Delta$, leads to flip of the dispersion $E \to -E$.

Now, defining the Fourier transform of the *total* Green's function at the two valleys, upon shifting to the Dirac points with $\mathbf{k} \to \mathbf{k} + \lambda\mathbf{K}$, we obtain the following expression for the components in real space

$$G_{\mu\nu}(\mathbf{r}_{ll'}, E; \phi) = \frac{\mathcal{A}}{(2\pi)^2} \sum_{\lambda=\pm 1} \int_{B.Z.} d^2\mathbf{k}\; G_{\mu\nu}(\mathbf{k}, E; \lambda; \phi) \mathrm{e}^{i(\mathbf{k}+\lambda\mathbf{K})\cdot\mathbf{r}_{ll'}}, \tag{4}$$

where the integration over the wave vector $\mathbf{k}$ is carried out in the Brillouin zone (B.Z.) and we have used $\mathbf{r}_{ll'} = \mathbf{r}_l - \mathbf{r}_{l'}$. After some straightforward algebra (see Appendix A) we obtain the Green's function tensor as a Hadamard product

$$\mathbf{G}(\mathbf{r}_{ll'}, E; \phi) = \frac{\mathcal{A}}{\pi a^2 E_0} \mathbf{V}^{1/2} \circ \mathbf{\Phi}^{1/2} \circ \mathbf{R}^{1/2}, \tag{5}$$

where the valley matrix is given by

$$\mathbf{V}^{1/2}(\mathbf{r}_{ll'}) = \begin{pmatrix} \cos(\mathbf{K}\cdot\mathbf{r}_{ll'}) & \sin(\mathbf{K}\cdot\mathbf{r}_{ll'} - \alpha_{ll'}) & \cos(\mathbf{K}\cdot\mathbf{r}_{ll'} - 2\alpha_{ll'}) \\ & \cos(\mathbf{K}\cdot\mathbf{r}_{ll'}) & \sin(\mathbf{K}\cdot\mathbf{r}_{ll'} - \alpha_{ll'}) \\ & & \cos(\mathbf{K}\cdot\mathbf{r}_{ll'}) \end{pmatrix},$$

and the α (or equivalently ϕ) dependent matrix has the form

$$\mathbf{\Phi}^{1/2} = \begin{pmatrix} \frac{\omega+\delta}{\omega-\omega_\delta}\left(1 - \frac{\omega-\delta}{\omega-\omega_\delta}\sin^2\phi\right) & \sqrt{\frac{\omega^2-\delta^2}{\omega(\omega-\omega_\delta)}}\frac{\omega+\delta}{\omega-\omega_\delta}\cos\phi & \frac{\omega^2-\delta^2}{(\omega-\omega_\delta)^2}\frac{\sin(2\phi)}{2} \\ & \frac{\omega^2-\delta^2}{\omega(\omega-\omega_\delta)} & \sqrt{\frac{\omega^2-\delta^2}{\omega(\omega-\omega_\delta)}}\frac{\omega-\delta}{\omega-\omega_\delta}\sin\phi \\ & & \frac{\omega-\delta}{\omega-\omega_\delta}\left(1 - \frac{\omega+\delta}{\omega-\omega_\delta}\cos^2\phi\right) \end{pmatrix}. \tag{6}$$

The position and energy dependent distance matrix is given by

$$\mathbf{R}^{1/2} = \omega \begin{pmatrix} -K_0(-i\Omega r) & -iK_1(-i\Omega r) & K_2(-i\Omega r) \\ & -K_0(-i\Omega r) & -iK_1(-i\Omega r) \\ & & -K_0(-i\Omega r) \end{pmatrix},$$

where $\Omega = \sqrt{\omega\frac{\omega^2-\delta^2}{\omega-\omega_\delta}}$, and the dimensionless length r is defined by $r = r_{ll'}a^{-1}$ with a denoting the AB separation on the lattice as shown in Fig. 1.

We now consider two magnetic impurities having spins $\mathbf{S}_1$ and $\mathbf{S}_2$ occupying the lattice sites $\mathbf{r}_l$ and $\mathbf{r}_{l'}$ respectively. The effective RKKY exchange interaction energy for this pair of spins in the sea of Dirac electrons is by linear response theory given in the Heisenberg form as

[23, 29, 30]

$$E_{\mu\nu}(r_{ll'};\phi) = \frac{\lambda_0^2\hbar^2}{4}\chi_{\mu\nu}\left(r_{ll'};\phi\right)\ \mathbf{S}_1\cdot\mathbf{S}_2\ ,$$

where λ_0 is the short-range exchange interaction between the impurity spins and the α-$\mathcal{T}_3$ electrons, and $\chi_{\mu\nu}\left(r_{ll'};\phi\right)$ is the free-particle charge density sublattice susceptibility which depends on the lattice sites $\mu,\nu = \mathtt{A},\mathtt{B},\mathtt{C}$ where the impurity spins are positioned and is given by

$$\chi_{\mu\nu}\left(r_{ll'};\phi,\delta,\mu\right) = -\frac{2}{\pi}\int_{-\infty}^{0} dE\ \mathtt{Im}\left[G^2_{\mu\nu}\left(E+i0^+\right)\right] \quad (7)$$

$$= \left(\frac{3\sqrt{3}}{2\pi E_0}\right)^2 E_0 V_{\mu\nu}\left(\mathbf{r}_{ll'}\right)\tilde{\chi}_{\mu\nu}\left(r_{ll'};\phi,\delta,\mu\right).$$

Here $\mu = E_F/E_0$ is a normalized Fermi energy. A new valley matrix is given by the highly oscillatory direct product $\mathbf{V} = \mathbf{V}^{1/2}\circ\mathbf{V}^{1/2}$.

We now focus on the dimensionless envelop matrix elements $\tilde{\chi}_{\mu\nu}$ given by

$$\tilde{\boldsymbol{\chi}} = -\frac{2}{\pi}\int_{-\infty}^{\mu} d\omega \mathtt{Im}\left[\boldsymbol{\Phi}\circ\mathbf{R}\right], \quad (8)$$

where $\boldsymbol{\Phi} = \boldsymbol{\Phi}^{1/2}\circ\boldsymbol{\Phi}^{1/2}$ is a smooth function of ω, and $\mathbf{R} = \mathbf{R}^{1/2}\circ\mathbf{R}^{1/2}$ is the oscillating kernel. It is convenient to separate the above expression writing

$$\tilde{\boldsymbol{\chi}} = \tilde{\boldsymbol{\chi}}^{(0)} + \tilde{\boldsymbol{\chi}}^{(1)} \quad (9)$$

$$= -\frac{2}{\pi}\int_{-\infty}^{-\mu} d\omega \mathtt{Im}\left[\boldsymbol{\Phi}\circ\mathbf{R}\right] - \frac{2}{\pi}\int_{-\mu}^{\mu} d\omega \mathtt{Im}\left[\boldsymbol{\Phi}\circ\mathbf{R}\right].$$

Note that due to the symmetry of the kernel the $\tilde{\boldsymbol{\chi}}^{(1)}(\delta = 0)$ term vanishes, therefore its contribution is a direct measure of the magnetic field influence. At this point we consider the high doping regime $\delta/\mu \ll 1$, so that we can neglect the δ-effect in

$$\tilde{\boldsymbol{\chi}}^{(0)} \simeq \tilde{\boldsymbol{\chi}}^{(0)}(\delta = 0) = -\frac{2}{\pi}\boldsymbol{\Phi}\circ\int_{-\infty}^{-\mu} d\omega \mathtt{Im}\left[\mathbf{R}\right]. \quad (10)$$

Its exact expression in terms of the Meijer G functions was first obtained in Ref. [15] and exhibits Friedel oscillations in the susceptibility.

The second contribution to the susceptibility in Eq.(9) was worked out numerically. Special attention has to be paid to the gap region $-\delta < \omega < \delta$ since it contains a singularity at $\omega = -\delta\cos(2\phi)$ which is the asymptotic of the middle (flat band) dispersion curve in Fig. 2. The Zeeman kernel $\mathtt{Im}\left[\boldsymbol{\Phi}\circ\mathbf{R}\right]$ becomes highly oscillatory upon approaching the singular point (see Fig. 1 in the supplementary material of [48]) and the integral was determined using

$$\int_{-\delta\cos(2\phi)}^{\delta} \cdots = \sum_i \int_{\omega_i}^{\omega_{i+1}} \cdots\ , \quad (11)$$

where ω_i are the kernel $\mathbf{R}$ zeroes in ascending order. The magnitude of the above summation grows with $r_{ll'}$. The kernel with and without Zeeman effect for small $k_F r$ is shown in Fig. 2 of the supplementary material. Note that along the $\mathtt{AC}$ direction the kernel singularity occurs even for $\delta = 0$. This is a manifestation of the flat band contribution. The Zeeman effect deforms the otherwise flat band and its contribution is pronounced in all magnetic impurities orientations.

In Fig. 3, we analyze the $\tilde{\boldsymbol{\chi}}^{(1)}$ elements. These are shifted to the right for $\delta > 0$ when compared to $\tilde{\boldsymbol{\chi}}^{(0)}$ for small values of $r_{ll'}$. The left shift occurs upon flipping of the magnetic field orientation $\delta \to -\delta$ following the flip in the dispersion curve $E \to -E$ (see Fig. 2). Let us focus on points in the lattice such that $\tilde{\boldsymbol{\chi}}^{(0)} = 0$. Switching orientation in the magnetic field changes the RKKY interaction from ferromagnetic to antiferromagnetic. This effect may be useful in spintronics. Another interesting effect occurs at larger $k_F r$ where the shift may disappear and change its direction in beats-like format. We may attribute the beats to the broken particle-hole symmetry where two types of Friedel oscillations occur. This is supported by the fact that the beats disappear upon restoring the symmetry to the lattice as in the dice lattice case of $\phi = \pi/4$ (see Fig. 7). It is also worthwhile noticing that the dice lattice gives vanishing $\chi^{(1)}_{AC}$.

The kernel plays a crucial role in the low temperature correction $k_bT/\mu \ll 1$ obtained in the Sommerfeld expansion [15]

$$\tilde{\boldsymbol{\chi}} = \tilde{\boldsymbol{\chi}}\left(T=0\right) + \frac{\pi^2}{6}\left(\frac{k_bT}{E_0}\right)^2 \tilde{\boldsymbol{\chi}}^{(2)}\left(\omega=\mu\right), \quad (12)$$

$$\tilde{\boldsymbol{\chi}}^{(2)} = \frac{d}{d\omega}\mathtt{Im}\left[\boldsymbol{\Phi}\circ\mathbf{R}\right].$$

It is clear that the expansion fails around a singular point and the edges of the gap (see Fig. 3 of the supplemental material). The standard approach to correct the expansion is to define a chemical potential that depends on temperature. This would take us beyond the scope of this investigation.

III. STRONG MAGNETIC FIELD EFFECTS ON THE RKKY INTERACTION. FORMATION OF LANDAU LEVELS

We performed our calculations using the Landau gauge, for which the vector potential is $\mathbf{A} = -B_z y\hat{x}$ and $\nabla\times\mathbf{A} = B_z\hat{z}$ is the magnetic field. Using the Hamiltonian of Eq. (1), one can determine the wave functions and Landau levels for the lattice. Making use of the vector

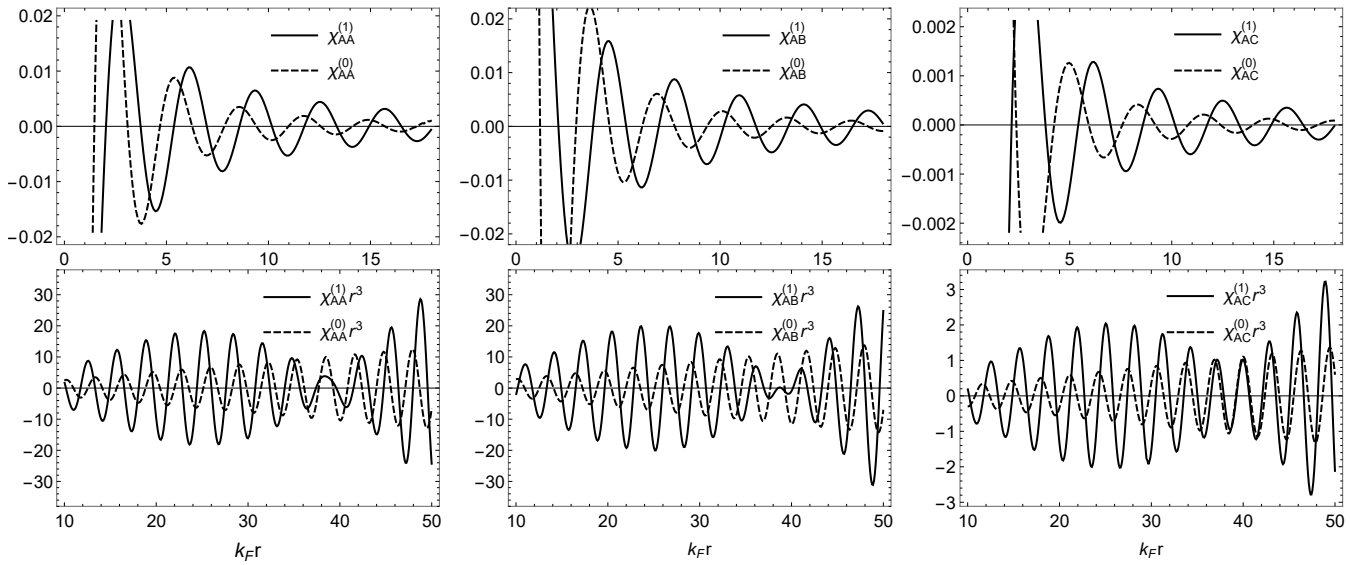

FIG. 3: Eq. (9) along various directions for small (top panel) and large (lower panel) distances and the set of numerical parameters $\phi = \pi/10$, $\delta = 0.1$, $\mu = 1.0$.

potential and the Peierls substitution $\hbar\mathbf{k} \to \mathbf{p} \to \mathbf{p} + e\mathbf{A}$, where $\hbar\mathbf{k}$ is the momentum eigenvalue in the absence of magnetic field and $\mathbf{p}$ is the momentum operator, we have

$$\begin{aligned} \hat{\mathbf{H}}_{\mathbf{K}} &= -\hat{\mathbf{H}}^{*}_{\mathbf{K}'} \qquad (13) \\ &= E_B \begin{pmatrix} 0 & \cos\phi\ \hat{a} & 0 \\ \cos\phi\ \hat{a}^{+} & 0 & \sin\phi\ \hat{a} \\ 0 & \sin\phi\ \hat{a}^{+} & 0 \end{pmatrix}, \end{aligned}$$

where $E_B = \sqrt{2}\gamma l_B^{-1}$ is the cyclotron energy related to the magnetic length $l_B = \sqrt{\hbar/(eB_z)}$. We also define the annihilation operator $\hat{a} = \dfrac{1}{\sqrt{2\hbar e B_z}}(\hat{p}_x - eB_z\hat{y} - i\hat{p}_y)$ and the creation operator $\hat{a}^{+} = \dfrac{1}{\sqrt{2\hbar e B_z}}(\hat{p}_x - eB_z\hat{y} + i\hat{p}_y)$ as in the case of the harmonic oscillator. We note that when $\phi = 0$, the Hamiltonian sub-matrix consisting of the first two rows and columns is the one used in [41, 42] for monolayer graphene.

In the most general case, let us denote the eigenstates by $\{\mathbf{\Psi_n}(\mathbf{r}), E_{\mathbf{n}}\}$, where the eigenfunctions are orthonormal, i.e., $\int d^2\mathbf{r}\mathbf{\Psi}^{T}_{\mathbf{n1}}(\mathbf{r})\,\mathbf{\Psi}^{\star}_{\mathbf{n2}}(\mathbf{r}) = \delta_{\mathbf{n1},\mathbf{n2}}$. We then write the Green's function as

$$\mathbf{G}(E;\mathbf{r}_{ll'}) = \frac{1}{E\mathbf{I} - \mathbf{H}} = \sum_{\mathbf{n}} \frac{\mathbf{\Psi}^{\star}_{\mathbf{n}}(\mathbf{r}_l)\,\mathbf{\Psi}^{T}_{\mathbf{n}}(\mathbf{r}_{l'})}{E - E_{\mathbf{n}} + i0^{+}}. \qquad (14)$$

In the presence of magnetic field, we have $\mathbf{n} = \{\lambda, s, n, k_y\}$, where $\lambda = \pm 1$ denotes the $\mathbf{K}$ or $\mathbf{K'} = -\mathbf{K}$ valley ; $s = -1, 0, 1$ stands for the valence, flat or conduction bands respectively; $n \geq 0$ is the Landau level index; and k_y is the wave vector. The energies can by found by diagonalizing the Hamiltonian (13) as

$$E_{\mathbf{n}} = E_B\epsilon_{\lambda,s,n} = E_B s\sqrt{n + \chi_\lambda}\ , \qquad (15)$$

where the auxiliary parameter $\chi_\lambda = [1 - \lambda\cos(2\phi)]/2$ with $0 \leq \chi_\lambda < 1$ has been used.

The susceptibility components at $T = 0$ K and the Fermi energy E_F are given by Eq. (7). Using the Green's function in Eq. (14) we obtain

$$\begin{aligned} \chi_{\mu\nu} &= -\frac{1}{\pi}\mathtt{Im}\int_{-\infty}^{\infty} dE\ \theta(E_F - E)\, G^2_{\mu\nu}(E;\mathbf{r}_{ll'}) \qquad (16) \\ &= -\frac{1}{\pi}\mathtt{Im}\sum_{\mathbf{n}_1,\mathbf{n_2}} \Psi^{\mu\nu}_{\mathbf{n}_1;\mathbf{n_2}}(\mathbf{r}_l,\mathbf{r}_{l'}) \int_{-\infty}^{\infty} dE\ \frac{\theta(E_F - E)}{(E_{\mathbf{n}_1} - E_{\mathbf{n}_2})} \\ &\quad \times \left(\frac{1}{E - E_{\mathbf{n}_1} + i0^{+}} - \frac{1}{E - E_{\mathbf{n}_2} + i0^{+}}\right) \\ &= \sum_{\mathbf{n}_1,\mathbf{n_2}} \Psi^{\mu\nu}_{\mathbf{n}_1;\mathbf{n_2}}(\mathbf{r}_l,\mathbf{r}_{l'}) \left[\frac{\theta(E_F - E_{\mathbf{n}_1}) - \theta(E_F - E_{\mathbf{n}_2})}{E_{\mathbf{n}_1} - E_{\mathbf{n}_2}}\right]. \end{aligned}$$

Here, we have used the shorthand notation $\Psi^{\mu\nu}_{\mathbf{n}_1;\mathbf{n_2}}(\mathbf{r}_l,\mathbf{r}_{l'}) = \Psi^{\star\mu}_{\mathbf{n}_1}(\mathbf{r}_l)\,\Psi^{\nu}_{\mathbf{n}_1}(\mathbf{r}_{l'})\,\Psi^{\star\mu}_{\mathbf{n}_2}(\mathbf{r}_{l'})\,\Psi^{\nu}_{\mathbf{n}_2}(\mathbf{r}_l)$.

Mapping the sites of the lattice $\mathtt{A,B,C} \to -1, 0, 1$ and separating the spatial variables in the wave function we obtain

$$\Psi^{\star\mu}_{\mathbf{n}}(\mathbf{r}_l) = \psi^{\mu}_{\lambda,s,n}\phi_{n+\lambda\mu,k_y}(x_l)\,\mathsf{e}^{-ik_y y_l}\mathsf{e}^{-i\lambda K_y y_l}, \qquad (17)$$

where the vector components specific to the given lattice are denoted by $\psi^{\mu}_{\lambda,s,n}$, $\phi_{n,k_y}(x_l)$ and are given by the harmonic oscillator wave functions. When $s^2 = 1$ these components take the following form

$$\psi^{\mu}_{\lambda,s,n} = \frac{1}{\sqrt{2(n + \chi_\lambda)}} \begin{cases} \sqrt{n(1-\chi_\lambda)}, & \lambda\mu = -1 \\ s\lambda\sqrt{(n+\chi_\lambda)}, & \lambda\mu = 0\ . \\ \sqrt{(n+1)\chi_\lambda}, & \lambda\mu = 1 \end{cases} \qquad (18)$$

For the flat band ($s = 0$) when $n > 0$ the components are

$$\psi^{\mu}_{\lambda,s,n} = \frac{1}{\sqrt{n+\chi_\lambda}} \begin{cases} -\lambda\sqrt{(n+1)\chi_\lambda}, & \lambda\mu = -1 \\ 0, & \lambda\mu = 0 \\ \lambda\sqrt{n(1-\chi_\lambda)}, & \lambda\mu = 1 \end{cases}, \quad (19)$$

while for $n = 0$ the components are

$$\psi^{\mu}_{\lambda,s,n} = \begin{cases} 0, & \lambda\mu = -1 \\ 0, & \lambda\mu = 0 \\ 1, & \lambda\mu = 1 \end{cases}. \quad (20)$$

By combining Eqs. (15), (16) and (18),and after some algebra (see Appendix B) we finally obtain the general form of the susceptibility components

$$\chi^{\mu\nu} = \frac{\mathcal{A}}{E_B\left(2\pi l_B\right)^2}\tilde{\chi}^{\mu\nu}\left(\mathbf{r}_l, \mathbf{r}_{l'}\right), \quad (21)$$

$$\tilde{\chi}^{\mu\nu}\left(\mathbf{r}_l, \mathbf{r}_{l'}\right) = \sum_{\lambda_{1,2}=\pm1}\sum_{s_{1,2}=0,\pm1}\sum_{n_{1,2}\geq 0}\psi^{\mu\nu}_{\lambda_1 s_1 n_1;\lambda_1 s_1 n_1}$$
$$\times\tilde{\Phi}^{n_1+\lambda_1\nu}_{n_1+\lambda_1\mu}\left(s_1;\mathbf{r}_l,\mathbf{r}_{l'}\right)\tilde{\Phi}^{n_2+\lambda_2\nu}_{n_2+\lambda_2\mu}\left(s_2;\mathbf{r}_{l'},\mathbf{r}_l\right)\mathrm{e}^{-iK(\lambda_1-\lambda_2)(y_l-y_{l'})}$$
$$\times\frac{\theta\left(\mu_F - s_1\sqrt{n_1+\chi_{\lambda_1}}\right) - \theta\left(\mu_F - s_2\sqrt{n_2+\chi_{\lambda_2}}\right)}{s_1\sqrt{n_1+\chi_{\lambda_1}} - s_2\sqrt{n_2+\chi_{\lambda_2}}},$$

where we have introduced the normalized Fermi energy $\mu_F = E_F/E_B$ as well as $\psi^{\mu\nu}_{\lambda_1 s_1 n_1;\lambda_1 s_1 n_1} = \psi^{\mu}_{\lambda_1,s_1,n_1}\psi^{\nu}_{\lambda_1,s_1,n_1}\psi^{\mu}_{\lambda_2,s_2,n_2}\psi^{\nu}_{\lambda_2,s_2,n_2}$. Equation (21) is applicable for a wide range of experimental parameters and serves as a basis for the numerical simulations which are presented below. For simplicity, we neglect highly oscillatory inter-valley terms setting $\lambda_1 = \lambda_2 = \lambda = \pm 1$.

Figure 4 presents the magnetic field dependent susceptibility as a function of the spin separation when $E_F = 0$ at $T = 0$ K. Three values of ϕ were chosen in the numerical calculations. They all show regions of ferromagnetic and antiferromagnetic behavior with the amplitude of the oscillations decreasing with increasing separation between the spins on the lattice. However, for $\phi = \pi/80$ in Fig. 4, $\chi_{\mathtt{CC}}$ has the largest amplitude for the oscillations and $\chi_{\mathtt{AB}} + \chi_{\mathtt{BA}}$, $\chi_{\mathtt{AC}} + \chi_{\mathtt{CA}}$ and $\chi_{\mathtt{BC}} + \chi_{\mathtt{BA}}$ all remain negative and independent of $r_{ll'}$. These results are interesting as they demonstrate how one could control the magnetic behavior of the α-$\mathcal{T}_3$ lattice. Most importantly, the results in Fig. 4 signal that the magnetic properties of the α-$\mathcal{T}_3$ lattice near $\alpha = 0$ need to be compared with those for graphene in Fig. 6. Remarkably, the susceptibility has one sign for small $r_{ll'}$. The component $\chi_{\mathtt{AA}}$ oscillates but remains positive for large spin separation. On the contrary, both $\chi_{\mathtt{AB}}$ and the sum $\chi_{\mathtt{AA}} + \chi_{\mathtt{AB}}$ remain negative in this limit. This behavior is independent of the position of the Fermi level. We point out that in doing the calculations for graphene, we *first* set $\alpha = 0$ in Eq. (13) before calculating the eigenstates which were in turn employed in the spin susceptibility. Therefore, the change in behavior discovered here is clear when α is finite and zero.

We now turn our attention to two specific cases where closed form analytic expressions can be obtained for the spin susceptibility. A very interesting case occurs when the lattice is undoped, i.e. $E_F = 0$, in strong magnetic field for which there are well separated Landau levels at $\lambda = 1$ and $\phi \to 0$. The dominant contributions to Eq. (21) comes from $n_{1,2} = 0$ terms

$$\tilde{\chi}^{\mu\nu} = \sum_{s_{1,2}=0,\pm1}\tilde{\Phi}^{\nu}_{\mu}\left(s_1;\mathbf{r}_l,\mathbf{r}_{l'}\right)\tilde{\Phi}^{\nu}_{\mu}\left(s_2;\mathbf{r}_{l'},\mathbf{r}_l\right) \quad (22)$$
$$\times\psi^{\mu}_{1,s_1,0}\psi^{\nu}_{1,s_1,0}\psi^{\mu}_{1,s_2,0}\psi^{\nu}_{1,s_2,0}\frac{\theta\left(-s_1\sin\phi\right) - \theta\left(-s_2\sin\phi\right)}{s_1\sin\phi - s_2\sin\phi}.$$

Let us introduce the normalized temperature $\tilde{T} = \frac{k_B T}{E_B}$ and the integral representation of the Fermi function instead of the θ function. For an arbitrarily chosen small temperature, we set $\tilde{T} = \sin^2(\phi)$, and we expand the above equation around small positive ϕ to obtain

$$\tilde{\chi}^{\mu\nu} \sim \frac{\mathtt{Erf}\left[\frac{1}{\sqrt{2}}\right]\mathtt{Exp}\left[\frac{-r^2_{ll'}}{2}\right]}{4\phi} \quad (23)$$
$$\times\left[\begin{pmatrix}0&0&0\\0&-1&1\\0&1&-1\end{pmatrix} + \begin{pmatrix}0&0&0\\0&0&0\\0&0&-4\end{pmatrix}\right].$$

The first matrix is due to transitions between the valence and conduction bands as well as within the conduction band from below to above the Fermi level. The second matrix arises from transitions from the flat band to the conduction band. We conclude from these results that the largest change in the spin susceptibility occurs in the limit when $\phi \to 0$ and there is no smooth transition from finite ϕ to $\phi = 0$. This in turn indicates that there is a phase transition between graphene ($\phi = 0$) and the α-$\mathcal{T}_3$ model. This anomaly is short range due to the exponent, and has no counterpart in the $\mathbf{K}$ ($\lambda = -1$) valley.

We also study the case of high doping when the Fermi level n_F is defined via

$$\sqrt{n_F - 1 + \chi_{\lambda_1}} \leq \mu_F \leq \sqrt{n_F + \chi_{\lambda_2}}.$$

In this case, there are only intraband $s_1 = s_2 = 1$ contributions to the susceptibility. The leading terms (largest contributions to the sum) come from the states nearest to n_F. Specifically, for large n_F, we found numerically that the terms in Eq. (21) scale as $\delta_{|n_1-n_2|,1}$. The transitions from the flat to the conduction band do not follow this rule, they rather scale as $\sim 1/n_F$ which allows us to neglect such contributions. A similar approach was adapted by Lozovik [44] when he discussed edge magnetoplasmons in graphene (leading contributions to the conductivity tensor in the above mentioned limit). However, there is an important difference in that the magnetoplasmons are given by the optical conductivity tensor where $\delta_{|n_1-n_2|,1}$ is the true selection rule which applies for all n.

In this limiting case Eq. (21) can be written in a compact form as

$$\tilde{\boldsymbol{\chi}} = [\mathbf{I} \circ \boldsymbol{\Phi}_{\lambda_1=\lambda_2} + \mathbf{V}_{\lambda_1=-\lambda_2} \circ \boldsymbol{\Phi}_{\lambda_1=-\lambda_2}] \circ \mathbf{R} \ . \tag{24}$$

Contributions from the same valley $\lambda_1 = \lambda_2$ (first term in the square brackets of the above expression) are given by $\boldsymbol{\Phi} = \boldsymbol{\Phi}^{1/2} \circ \boldsymbol{\Phi}^{1/2}$ which is identical to the no-magnetic field case $\delta = 0$ in Eq. (6),

$$\boldsymbol{\Phi}_{\lambda_1=\lambda_2} = \begin{pmatrix} \cos^4\phi & \cos^2\phi & \frac{1}{4}\sin^2 2\phi \\ & 1 & \sin^2\phi \\ & & \sin^4\phi \end{pmatrix} . \tag{25}$$

However, for mixed valley contributions, $\lambda_1 = -\lambda_2$, we obtain highly oscillatory terms $\mathbf{V}_{\lambda_1=-\lambda_2} = \cos(2Ky_{ll'})\mathbf{I}$ along with a peculiar form for the $\phi-$matrix

$$\boldsymbol{\Phi}_{\lambda_1=-\lambda_2} = \begin{pmatrix} \frac{1}{4}\cot^2\phi & \frac{1}{2}\csc^2\phi & -2 \\ & \csc^2(2\phi) & \frac{1}{2}\sec^2\phi \\ & & \frac{1}{4}\tan^2\phi \end{pmatrix} . \tag{26}$$

It is informative to look at the upper-left 2×2 sub-matrix in Eqs. (25) and (26) corresponding to the graphene like case of `A` and `B` sub-lattices. While Eq. (25) provides smooth transition to graphene at $\phi \to 0$, the valley mixing in Eq. (26) gives $1/\phi^2$ scaling. The absence of the smooth graphene limit can be directly attributed to broken symmetry for the $\mathbf{K}$ and $\mathbf{K}'$ valleys in magnetic field.

The site-to-site distance and Fermi number dependent matrix referred to Eq. (24) is given by

$$\mathbf{R}(r_{ll'}, n_F) = \frac{1}{2\pi r} \begin{pmatrix} -4\cos^2\left(2\sqrt{n_F}r\right) & e^{-r^2}\cos\left(4\sqrt{n_F}r\right) + 1 & \frac{1}{4}\left[e^{-r^2}\cos\left(4\sqrt{n_F}r\right) + 1\right] \\ & -4\cos^2\left(2\sqrt{n_F}r\right) & e^{-r^2}\cos\left(4\sqrt{n_F}r\right) + 1 \\ & & -4\cos^2\left(2\sqrt{n_F}r\right) \end{pmatrix} , \tag{27}$$

where for convenience we have omitted the subscripts through the replacement $r_{ll'}/\sqrt{2} \to r$. If we formally associate $\sqrt{n_F}$ with k_F, the oscillations in the above equation correspond to Kohn anomalies in the absence of magnetic field which was first reported in Ref. [35]. However, they are much larger in range due to the $\sim 1/r$ dependence. At larger distances, we can neglect the terms $\sim \exp(-r^2)$ and the oscillations for impurities which are placed on different sub-lattices vanish.

IV. CONCLUDING REMARKS AND SUMMARY

We have investigated the behavior of the RKKY interaction for undoped and doped α-$\mathcal{T}_3$ semi-metals as well as when they are subjected to a uniform perpendicular magnetic field. Specifically, we have shown the following: (a) For undoped samples, the RKKY interaction obeys an inverse cubic law for the separation between spins located on lattice sites. The strength of this interaction is anisotropic and determined by the adjustable hopping parameter ϕ except when both spins are on `B` sites. Furthermore, the `AA`, `BB` and `CC` exchange interactions are ferromagnetic but the sign of this interaction is reversed when the spins are located on different sublattices; (b) for the case when the chemical potential is finite, we were able to express our closed form analytic expression for the spin susceptibility in the same algebraic form as in case (a). However, the amplitudes of these interactions are multiplied by an oscillatory factor which could be positive or negative for ranges of the spin separations; (c) in the presence of magnetic field, the spin susceptibility oscillates as the spin separation is varied displaying ranges of ferromagnetism and antiferromagnetism. When ϕ is small, we found that the behavior of the susceptibility is radically different compared to when the dice or Lieb phase ($\phi = \pi/4$) is approached. These observations confirm that a phase transition occurs as $\phi \to 0$ and this phase change is signaled through an applied magnetic field. A phase change was also reported in Ref. [47] when it was discovered the softening of a magnetoplasmon mode as the hopping parameter is reduced; (d) we were able to obtain analytic expressions for the spin susceptibility in the limit of low magnetic field or high doping. Interestingly, the power law behavior as a function of spin separation is $\sim 1/r$ which is a new result reported here. At large distances between the impurities the RKKY interaction exhibits Kohn anomalies only when those are located on the same sub-lattices. These effects are experimentally observable signatures of the electronic properties of α-$\mathcal{T}_3$ semi-metals and could serve to motivate others to apply them to future technologies.

Acknowledgement(s)

G.G. would like to acknowledge the support from the Air Force Research Laboratory (AFRL) through Grant No. FA9453-21-1-0046

Appendix A: Derivation of Eq. (5)

Here, we obtain analytical form of the following integral in Eq. (4)

$$\sum_{\lambda} \int_{B.Z.} \cdots \approx \sum_{\lambda} \int_{0}^{\infty} dk \int_{0}^{2\pi} d\theta = \sum_{\lambda} \int\int , \qquad \text{(A1)}$$

where the upper limit of the k integral is extended to ∞ and we used $\theta_k = \theta + \alpha_{ll'}$ with $\alpha_{ll'}$ the angle which $\mathbf{r}_{ll'}$ makes with the positive k_x-axis. This leads to

$$\begin{aligned}
G_{\mathtt{AA}} &= \frac{2\mathcal{A}}{(2\pi)^2} \cos(\mathbf{K}\cdot\mathbf{r}_{ll'}) \int\int \frac{E(E+\Delta) - \epsilon_k^2 \sin^2\phi}{\mathcal{D}} \mathsf{e}^{i\mathbf{k}\cdot\mathbf{r}_{ll'}} \ , \\
G_{\mathtt{BB}} &= \frac{2\mathcal{A}}{(2\pi)^2} \cos(\mathbf{K}\cdot\mathbf{r}_{ll'}) \int\int \frac{E^2 - \Delta^2}{\mathcal{D}} \mathsf{e}^{i\mathbf{k}\cdot\mathbf{r}_{ll'}} \ , \\
G_{\mathtt{CC}} &= \frac{2\mathcal{A}}{(2\pi)^2} \cos(\mathbf{K}\cdot\mathbf{r}_{ll'}) \int\int \frac{E(E-\Delta) - \epsilon_k^2 \cos^2\phi}{\mathcal{D}} \mathsf{e}^{i\mathbf{k}\cdot\mathbf{r}_{ll'}} \ , \\
G_{\mathtt{AB}} &= \frac{\mathcal{A}}{(2\pi)^2} \left[\mathsf{e}^{i(\mathbf{K}\cdot\mathbf{r}_{ll'} - \alpha_{ll'})} \int\int \frac{(E+\Delta)\epsilon_k \cos\phi}{\mathcal{D}} \mathsf{e}^{i(\mathbf{k}\cdot\mathbf{r}_{ll'} - \theta)} \right. \\
&- \left. \mathsf{e}^{-i(\mathbf{K}\cdot\mathbf{r}_{ll'} - \alpha_{ll'}))} \int\int \frac{(E+\Delta)\epsilon_k \cos\phi}{\mathcal{D}} \mathsf{e}^{i(\mathbf{k}\cdot\mathbf{r}_{ll'} + \theta)} \right] \ , \\
G_{\mathtt{AC}} &= \frac{\mathcal{A}}{(2\pi)^2} \left[\mathsf{e}^{i(\mathbf{K}\cdot\mathbf{r}_{ll'} - 2\alpha_{ll'})} \int\int \frac{\epsilon_k^2 \sin(2\phi)}{2E(E^2 - \epsilon_k^2)} \mathsf{e}^{i(\mathbf{k}\cdot\mathbf{r}_{ll'} - 2\theta)} \right. \\
&+ \left. \mathsf{e}^{-i(\mathbf{K}\cdot\mathbf{r}_{ll'} - 2\alpha_{ll'})} \int\int \frac{\epsilon_k^2 \sin(2\phi)}{2E(E^2 - \epsilon_k^2)} \mathsf{e}^{i(\mathbf{k}\cdot\mathbf{r}_{ll'} + 2\theta)} \right] , \\
G_{\mathtt{BC}} &= \frac{\mathcal{A}}{(2\pi)^2} \left[\mathsf{e}^{i(\mathbf{K}\cdot\mathbf{r}_{ll'} - \alpha_{ll'})} \int\int \frac{(E-\Delta)\epsilon_k \sin\phi}{\mathcal{D}} \mathsf{e}^{i(\mathbf{k}\cdot\mathbf{r}_{ll'} - \theta)} \right. \\
&- \left. \mathsf{e}^{-i(\mathbf{K}\cdot\mathbf{r}_{ll'} - \alpha_{ll'})} \int\int \frac{(E-\Delta)\epsilon_k \sin\phi}{\mathcal{D}} \mathsf{e}^{i(\mathbf{k}\cdot\mathbf{r}_{ll'} + \theta)} \right] .
\end{aligned}$$

The above expressions can also be written in the form

$$\begin{aligned}
G_{\mathtt{AA}} &= \cos(\mathbf{K}\cdot\mathbf{r}_{ll'})\, F_{\mathtt{AA}}(\mathbf{r}_{ll'}, E; \phi), \\
G_{\mathtt{BB}} &= G_{\mathtt{AA}}(\mathbf{r}_{ll'}, E; \phi = 0), \\
G_{\mathtt{CC}} &= G_{\mathtt{AA}}(\mathbf{r}_{ll'}, E; \phi + \pi/2), \\
G_{\mathtt{AB}} &= \sin(\mathbf{K}\cdot\mathbf{r}_{ll'} - \alpha_{ll'})\, F_{\mathtt{AB}}(\mathbf{r}_{ll'}, E; \phi), \\
G_{\mathtt{AC}} &= \cos(\mathbf{K}\cdot\mathbf{r}_{ll'} - 2\alpha_{ll'})\, F_{\mathtt{AC}}(\mathbf{r}_{ll'}, E; \phi), \\
G_{\mathtt{BC}} &= \sin(\mathbf{K}\cdot\mathbf{r}_{ll'} - \alpha_{ll'})\, F_{\mathtt{BC}}(\mathbf{r}_{ll'}, E; \phi) \ . \qquad \text{(A2)}
\end{aligned}$$

Let us define the following auxiliary quantities given by the Hankel transforms

$$
\begin{aligned}
F_{\mathtt{AA}} &= \left(\frac{\mathcal{A}}{\pi a^2 E_0}\right)\int_0^\infty dq\ q\ J_0\left(qr\right)\left\{\frac{\omega\left(\omega+\delta\right)-q^2\sin^2\phi}{\omega\left(\omega^2-\delta^2\right)-\left[\omega+\delta\cos(2\phi)\right]q^2}\right\} \\
&= -\left(\frac{\mathcal{A}}{\pi a^2 E_0}\right)\omega K_0\left(-ir\sqrt{\frac{\omega\left(\omega^2-\delta^2\right)}{\omega+\delta\cos(2\phi)}}\right)\frac{\omega+\delta}{\omega+\delta\cos(2\phi)}\left[1-\frac{\omega-\delta}{\omega+\delta\cos(2\phi)}\sin^2\phi\right]\ , \\
F_{\mathtt{AB}} &= -\left(\frac{\mathcal{A}}{\pi a^2 E_0}\right)\int_0^\infty dq\ q\ J_1\left(qr\right)\left\{\frac{\left(\omega+\delta\right)q\cos\phi}{\omega\left(\omega^2-\delta^2\right)-\left[\omega+\delta\cos(2\phi)\right]q^2}\right\} \\
&= -i\left(\frac{\mathcal{A}}{\pi a^2 E_0}\right)\omega K_1\left(-ir\sqrt{\frac{\omega\left(\omega^2-\delta^2\right)}{\omega+\delta\cos(2\phi)}}\right)\sqrt{\frac{\omega^2-\delta^2}{\omega\left[\omega+\delta\cos(2\phi)\right]}}\frac{\omega+\delta}{\omega+\delta\cos(2\phi)}\cos\phi\ , \\
F_{\mathtt{AC}} &= \left(\frac{\mathcal{A}}{\pi a^2 E_0}\right)\int_0^\infty dq\ q\ J_2\left(qr\right)\left\{\frac{q^2}{\omega\left(\omega^2-\delta^2\right)-\left[\omega+\delta\cos(2\phi)\right]q^2}\right\}\frac{\sin(2\phi)}{2} \\
&= \left(\frac{\mathcal{A}}{\pi a^2 E_0}\right)\omega K_2\left(-ir\sqrt{\frac{\omega\left(\omega^2-\delta^2\right)}{\omega+\delta\cos(2\phi)}}\right)\frac{\omega^2-\delta^2}{\left[\omega+\delta\cos(2\phi)\right]^2}\frac{\sin(2\phi)}{2}\ , \\
F_{\mathtt{BB}} &= -\left(\frac{\mathcal{A}}{\pi a^2 E_0}\right)\omega K_0\left(-ir\sqrt{\frac{\omega\left(\omega^2-\delta^2\right)}{\omega+\delta\cos(2\phi)}}\right)\frac{\omega^2-\delta^2}{\omega\left[\omega+\delta\cos(2\phi)\right]}\ , \\
F_{\mathtt{CC}} &= -\left(\frac{\mathcal{A}}{\pi a^2 E_0}\right)\omega K_0\left(-ir\sqrt{\frac{\omega\left(\omega^2-\delta^2\right)}{\omega+\delta\cos(2\phi)}}\right)\frac{\omega-\delta}{\omega+\delta\cos(2\phi)}\left[1-\frac{\omega+\delta}{\omega+\delta\cos(2\phi)}\cos^2\phi\right]\ , \\
F_{\mathtt{BC}} &= -i\left(\frac{\mathcal{A}}{\pi a^2 E_0}\right)\omega K_1\left(-ir\sqrt{\frac{\omega\left(\omega^2-\delta^2\right)}{\omega+\delta\cos(2\phi)}}\right)\sqrt{\frac{\omega^2-\delta^2}{\omega\left[\omega+\delta\cos(2\phi)\right]}}\frac{\omega-\delta}{\omega+\delta\cos(2\phi)}\sin\phi\ .
\end{aligned}
\tag{A3}
$$

Here, we employed the well known integral

$$
\int_0^\infty dx\ \frac{x^{n+1}}{x^2+C^2}J_n(xR)=C^n\ K_n(-CR)\ ,
$$

where $K_n(x)$ $(n=0,1,2,\cdots)$ is a modified Bessel function of the second kind. Together Eqs. (A2) and (A3) yield the desired final expression.

Appendix B: Derivation of Eq. (21)

The integration over k_y in Eq. (16) can be performed analytically using

$$
\sum_{k_y}=\frac{\mathcal{A}}{2\pi}\int_{-\infty}^{\infty}\frac{d\left[Y+\left(x_{l'}+x_l\right)/2+i\left(y_{l'}-y_l\right)/2\right]}{2\pi l_B^2}\ , \tag{B1}
$$

then the expression for the wave functions overlap becomes

$$
\begin{aligned}
&\Phi_{n+\lambda\mu}^{n+\lambda\nu}\left(\mathbf{r}_l,\mathbf{r}_{l'}\right) \\
&=\sum_{k_y}\phi_{n+\lambda\mu,k_y}\left(x_l\right)\phi_{n+\lambda\nu,k_y}\left(x_{l'}\right)\mathsf{e}^{-ik_y\left(y_l-y_{l'}\right)} \\
&=\frac{\mathcal{A}}{2\pi}\frac{\exp\left[-\frac{r_{ll'}^2}{4}-i\frac{\left(x_l+x_{l'}\right)\left(y_l-y_{l'}\right)}{2l_B^2}\right]}{2\pi^{3/2}l_B^2\sqrt{2^{n+\lambda\mu}\left(n+\lambda\mu\right)!}\sqrt{2^{n+\lambda\nu}\left(n+\lambda\nu\right)!}} \\
&\times\int_{-\infty}^{\infty}dy\mathsf{e}^{-y^2}H_{n+\lambda\mu}\left(x-y\right)H_{n+\lambda\nu}\left(z-y\right)\ ,
\end{aligned}
\tag{B2}
$$

where $Y=k_y l_B^2$; $y=Y/l_B$; $x=\frac{\left(x_l-x_{l'}\right)+i\left(y_l-y_{l'}\right)}{2l_B}=\frac{r_{ll'}}{2}\exp\left(i\alpha_{ll'}\right)$; $z=\frac{\left(x_{l'}-x_l\right)+i\left(y_l-y_{l'}\right)}{2l_B}=-\frac{r_{ll'}}{2}\exp\left(-i\alpha_{ll'}\right)$ and $r_{ll'}=2|x|=2|z|$.

Now, let us use the following integral relation

$$\int_{-\infty}^{\infty} dy\ \mathtt{e}^{-y^2} H_{n+\lambda\mu}(x-y)\, H_{n+\lambda\nu}(z-y) \qquad \text{(B3)}$$

$$= \sqrt{\pi} 2^n \begin{cases} 2^{\lambda\nu}\,(n+\lambda\mu)!\ z^{\lambda(\nu-\mu)} L_{n+\lambda\mu}^{\lambda(\nu-\mu)}\left(\frac{r_{ll'}^2}{2}\right) & ;\ \lambda\mu \le \lambda\nu \\ 2^{\lambda\mu}\,(n+\lambda\nu)!\ x^{\lambda(\mu-\nu)} L_{n+\lambda\nu}^{\lambda(\mu-\nu)}\left(\frac{r_{ll'}^2}{2}\right) & ;\ \lambda\mu > \lambda\nu\ . \end{cases}$$

Including the flat band to the overlap function, we finally obtain

$$\Phi_{n+\lambda\mu}^{n+\lambda\nu}(s;\mathbf{r}_l,\mathbf{r}_{l'}) = \frac{\mathcal{A}}{(2\pi l_B)^2}\tilde{\Phi}_{n+\lambda\mu}^{n+\lambda\nu}(s;\mathbf{r}_l,\mathbf{r}_{l'})\,, \qquad \text{(B4)}$$

$$\tilde{\Phi}_{n+\lambda\mu}^{n+\lambda\nu}(s,\mathbf{r}_l,\mathbf{r}_{l'}) = \exp\left[-\frac{r_{ll'}^2}{4} - i\frac{(x_l+x_{l'})(y_l-y_{l'})}{2l_B^2}\right]\times$$

$$\begin{cases} \sqrt{\frac{2^{\lambda\nu}(n+\lambda\mu)!}{2^{\lambda\mu}(n+\lambda\nu)!}}\, z^{\lambda(\nu-\mu)} L_{n+\lambda\mu}^{\lambda(\nu-\mu)}\left(\frac{r_{ll'}^2}{2}\right) & ;\text{for } \lambda\mu \le \lambda\nu \\ \sqrt{\frac{2^{\lambda\mu}(n+\lambda\nu)!}{2^{\lambda\nu}(n+\lambda\mu)!}}\, x^{\lambda(\mu-\nu)} L_{n+\lambda\nu}^{\lambda(\mu-\nu)}\left(\frac{r_{ll'}^2}{2}\right) & ;\ \lambda\mu > \lambda\nu \\ 0 & ;\ n+\mathtt{min}(\lambda\mu,\lambda\nu) < 0 \\ L_0^0\left(\frac{r_{ll'}^2}{2}\right) & ;\ n=0, s=0\ . \end{cases}$$

Substituting Eqs. (18) and (B4) into Eq. (17) and the resulting equation into Eq. (16), we finally obtain Eq. (21).

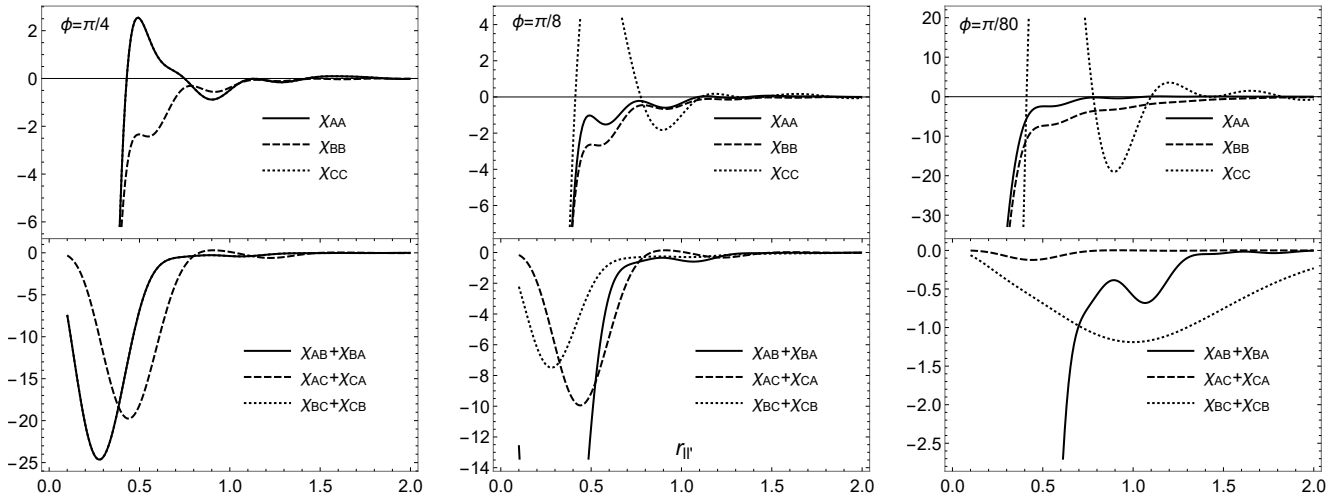

FIG. 4: Spin susceptibility in units of $\mathcal{A}/E_B\,(2\pi l_B)^2$ as a function of the inter-particle separation for $E_F = 0,\ T = 0$ K.

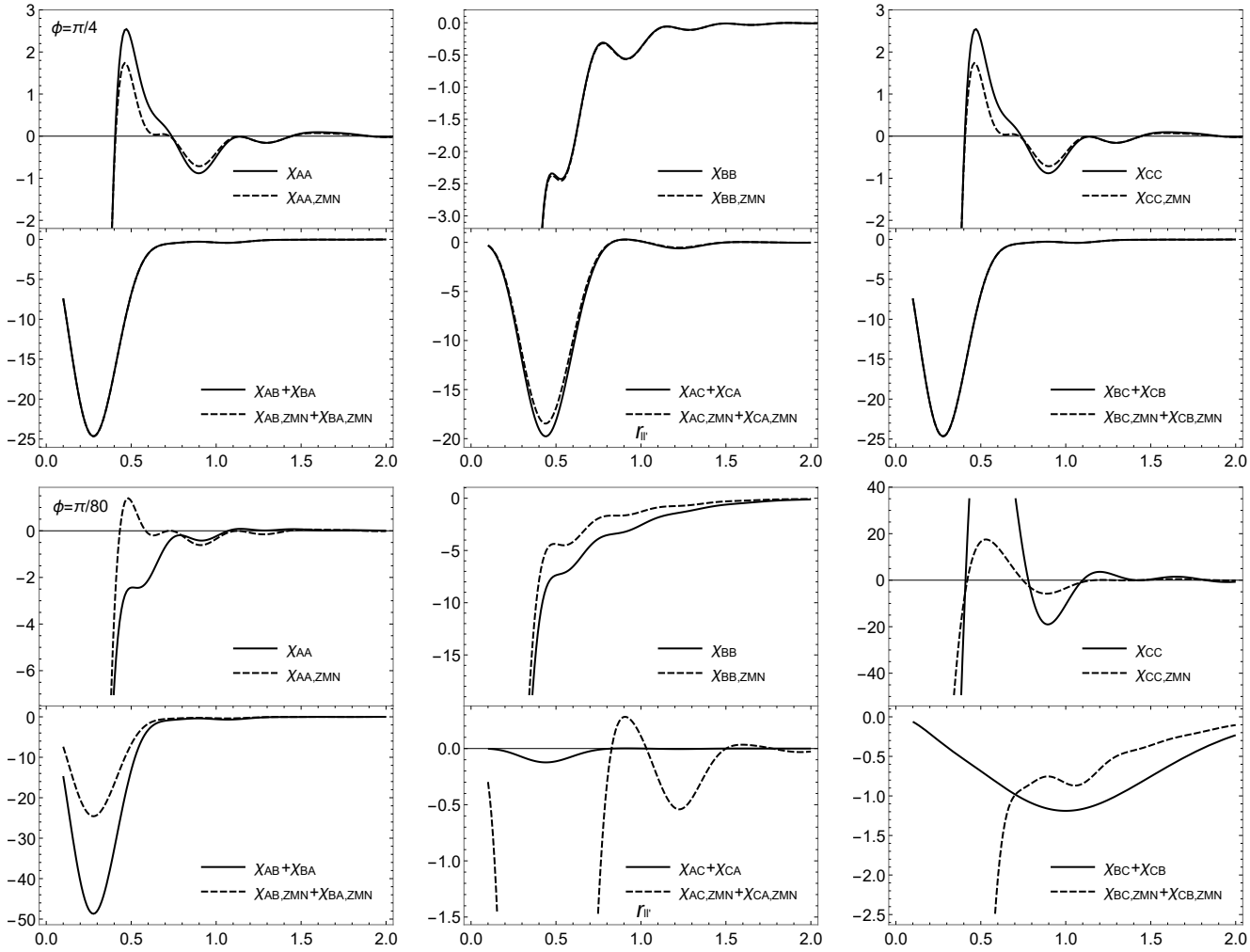

FIG. 5: Spin susceptibility as a function of the inter-particle separation for $E_F = 0,\ T = 0$ K.

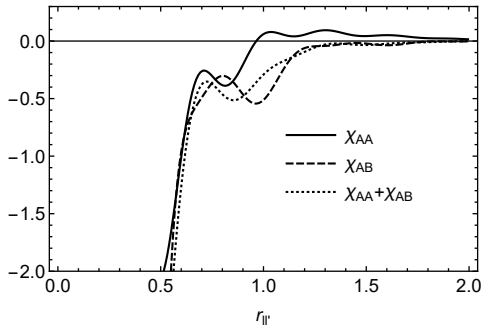

FIG. 6: Spin susceptibility of graphene as a function of the inter-particle separation for graphene with $E_F = 0$, $T = 0$ K.

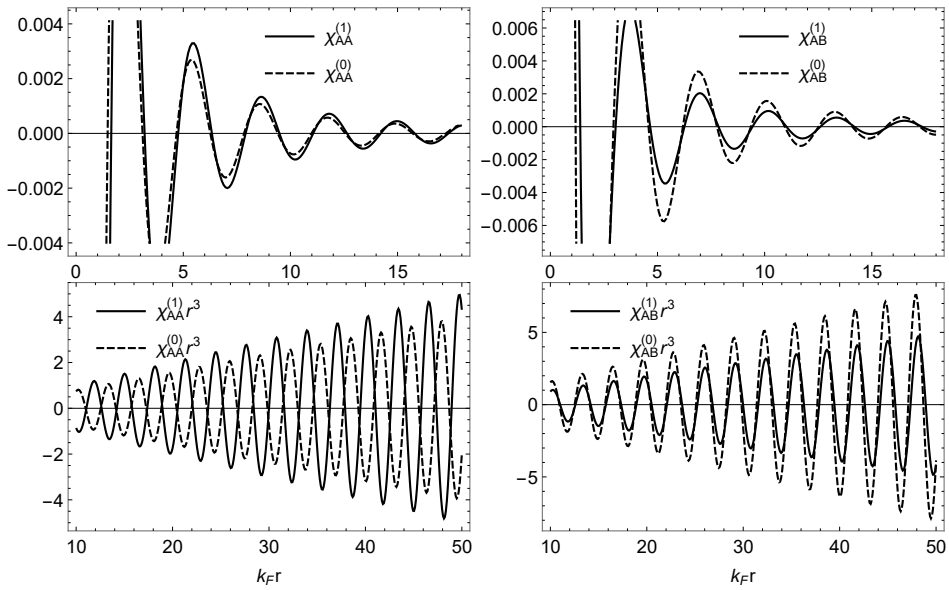

FIG. 7: Eq.(9) along various directions for small (top panel) and large (lower panel) distances and the set of numerical parameters $\phi = \pi/4$, $\delta = 0.1$, $\mu = 1.0$.

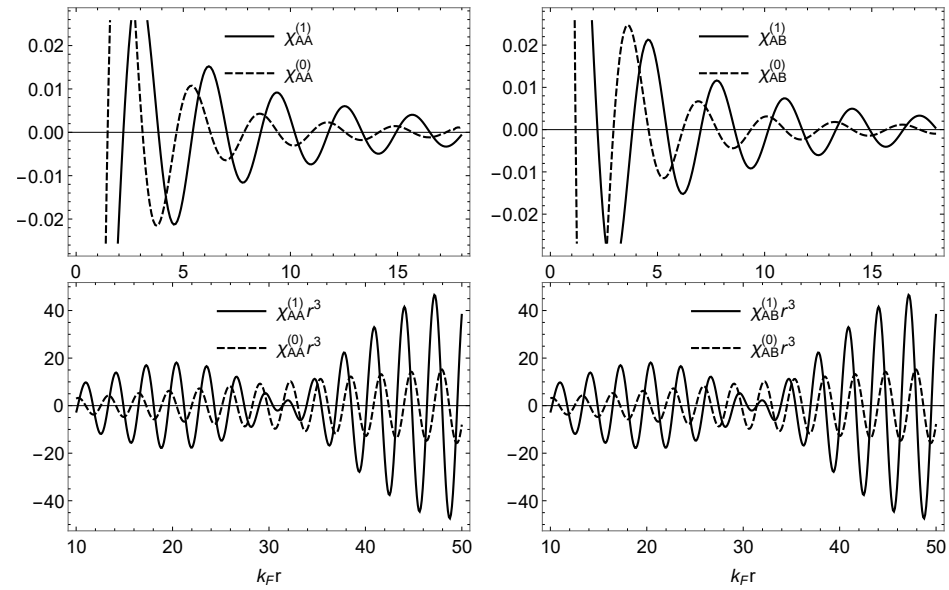

FIG. 8: Eq.(9) along various directions for small (top panel) and large (lower panel) distances and the set of numerical parameters $\phi = 0$, $\delta = 0.1$, $\mu = 1.0$.

[1] Daniel Leykam, Alexei Andreanov, and Sergej Flach, Advances in Physics: X, **3**, 1473052 (2018).
[2] A. Raoux, M. Morigi, J.-N. Fuchs, F. Piéchon, and G. Montambaux, Phys. Rev. Lett. **112**, 026402 (2014).
[3] B. Sutherland, Phys. Rev. B **34**, 5208 (1986).
[4] E. Illes, J. P. Carbotte, and E. J. Nicol Phys. Rev. B **92**, 245410 (2015).
[5] S. K. F. Islam and P. Dutta, Phys. Rev. B **96**, 045418 (2017).
[6] E. Illes and E. J. Nicol, Phys. Rev. B **94**, 125435 (2016).
[7] J. D. Malcolm and E. J. Nicol, Phys. Rev. B **93**, 165433 (2016).
[8] B. Dey and T. K. Ghosh, Phys. Rev. B **98**, 075422 (2018).
[9] G.-B. Jo, J. Guzman, C. K. Thomas, P. Hosur, A. Vishwanath, and D. M. Stamper-Kurn, Phys. Rev. Lett. **108**, 045305 (2012).
[10] F. Wang and Y. Ran, Phys. Rev. B **84**, 241103(R) (2011).
[11] B. Dey, P. Kapri, O. Pal and T. K. Ghosh, Phys. Rev. **B 101**, 235406 (2020).
[12] T. Biswas and T. K. Ghosh, J. Phys. Condens. Matter **30**, 075301 (2018).
[13] A. D. Kovacs, G. David, B. Dora, and J. Cserti, Phys. Rev. B **95**, 035414 (2017).
[14] T. Biswas and T. K. Ghosh, J. Phys. Condens. Matter **28**, 495302 (2016).
[15] D. O. Oriekhov and V. P. Gusynin, Phys. Rev. B **101**, 235162 (2020).
[16] J. Vidal, R. Mosseri, and B. Doucot, Phys. Rev. Lett. **81**, 5888 (1998).
[17] J. Vidal, P. Butaud, B. Doucot, and R. Mosseri, Phys. Rev. B **64**, 155306 (2001).
[18] B. Doora, J. Kailasvuori, and R. Moessner, Phys. Rev. B **84**, 195422 (2011).
[19] D. Huang, A. Iurov, H.-Y. Xu, Y.-C. Lai, and G. Gumbs, Phys. Rev. B **99**, 245412 (2019).
[20] Y. Li, S. Kita, P. Munoz, O. Reshef, D. I. Vulis, M. Yin, M. Loncar, and E. Mazur, Nat. Photonics **9**, 738 (2015).
[21] H.-Y. Xu, L. Huang, D. H. Huang, and Y.-C. Lai, Phys. Rev. B **96**, 045412 (2017).
[22] Bashab Dey and Tarun Kanti Ghosh, Phys. Rev. B **99**, 205429 (2019).
[23] M. Sherafati and S. Satpathy, Phys. Rev. B **84**, 125416 (2011).
[24] M. A. Ruderman and C. Kittel, Phys. Rev. **96**, 99 (1954).
[25] T. Kasuya, Prog. Theor. Phys. **16**, 45 (1956).
[26] K. Yosida, Phys. Rev. **106**, 893 (1957).
[27] J. Klinovaja and D. Loss, Phys. Rev. B **87**, 045422 (2013).
[28] M. Ke, M. M. Asmar, and WK. Tse, Phys. Rev. Research 2, 033228 (2020).
[29] O. Roslyak, G. Gumbs, and D. Huang, J. Appl. Phys. **113**, 123702 (2013).
[30] E. Kogan, Graphene **2**, 8 (2013).
[31] E. Kogan, Phys. Rev. B **. 84**, 115119 (2011).
[32] B. Uchoa, T. G. Rappoport, and A. H. Castro Neto, Phys. Rev. Let. **106**, 016801 (2011).
[33] M. Sherafati and S. Satpathy, Phys. Rev. B **83**, 165425 (2011).
[34] A. M. Black-Schaffer, Phys. Rev. B **81**, 205416 (2010).
[35] L. Brey, H. A. Fertig, and S. Das Sarma, Phys. Rev. Lett. **99**, 116802 (2007).
[36] S. Saremi, Phys. Rev. B **76**, 184430 (2007).
[37] V. K. Dugaev,V. I. Litvinov, and J. Barnas, Phys. Rev. B **74**, 224438 (2006).
[38] M. A. H. Vozmediano, M. P. Lopez-Sancho, T. Stauber, and F. Guinea, Phys. Rev. B **72**, 155121 (2005).
[39] J. Cao, H. A. Fertig, and S. Zhang, Phys. Rev. B **99**, 205430 (2019).
[40] Moslem Zare, Phys. Rev. B **100**, 085434 (2019).
[41] O. L. Berman, Y. E. Lozovik, and G. Gumbs, Phys. Rev. B **77**, 155433 (2008).
[42] R. Roldan, J.-N. Fuchs, and M. O. Goerbig, Phys. Rev. B **80**, 085408 (2009).
[43] A. Iurov, G. Gumbs, O. Roslyak, and D. Huang, J. Phys. Condens. Matter **25**, 135502 (2013).
[44] A. Sokolik and Y. E. Lozovik, Phys. Rev. B **100**, 125409 (2019).
[45] Romhányi, Judit and Penc, Karlo and Ganesh, Ramachandran, Nature Communications **6**, 1 (2015).
[46] E. V. Gorbar, V. P. Gusynin and D. O. Oreikhov, phys. Rev. B, **99**, 155124 (2019).
[47] A. Balassis, D. Dahal, G. Gumbs, A. Iurov, D. Huang, and O. Roslyak, J. Phys. Condens. Matter **32**, 485301 (2020).
[48] available online